RESEARCH ARTICLE | AUGUST 20 2014

Whispering gallery micro-global positioning system for nanoparticle sizing in real time FREE

D. Keng; X. Tan; S. Arnold

Appl. Phys. Lett. 105, 071105 (2014)
https://doi.org/10.1063/1.4893762
CHORUS

Whispering gallery micro-global positioning system for nanoparticle sizing in real time

D. Keng, X. Tan, and S. Arnold[a)]
Microparticle Photophysics Lab (MP³L), NYU Polytechnic School of Engineering, Brooklyn, New York 11201, USA

(Received 15 July 2014; accepted 11 August 2014; published online 20 August 2014)

We have devised a simple means for determining the size of a nanoparticle in one binding event (i.e., real time) by utilizing two polar modes of a slightly eccentric Whispering Gallery Mode (WGM) spheroidal resonator. The ratio of shifts of these modes locates the absolute latitude angle at which a nano-particle binds. From this location, the size of the nanoparticle is calculated using the reactive sensing principle. Although our latitude-only micro-global positioning scheme is applied to nanoparticle sizing using slightly eccentric spheroids in aqueous solution, this approach can be applied to WGM micro-resonators having a variety of shapes. © *2014 AIP Publishing LLC*.
[http://dx.doi.org/10.1063/1.4893762]

A quantitative bio-size/mass spectrometer that can work in solution, and work at single nanoparticle sensitivity, would have the possibility of adding important information to body fluid analysis. Furthermore, label-free sensors with this capability could identify viruses and exosomes not only by using bound antibodies but also through their size.

At present, determining the size of a nanoparticle in one event by using an optical micro-resonator has required a high Q WGM resonator ($Q \sim 10^7$–10^8) and a combination of a reactive splitting $2g$, and an increase in linewidth $\Delta\Gamma$ associated with light scattering.[1] The splitting is caused by lifting the clockwise-counterclockwise degeneracy associated with orbiting photons within WGMs. Whereas the splitting is proportional to the polarizability α of the adsorbing nanoparticle, which is, in turn, proportional to the particle volume, the increase in linewidth is proportional to α^2, so that the ratio $\Delta\Gamma/(2g)$ can be used to obtain the polarizability, and from that the particle size/mass. However, the splitting vanishes if it is smaller than the cavity linewidth, thereby setting a lower limit for the detectable nanoparticle size.[2] The resulting degenerate mode still shifts, but it is only possible to obtain the polarizability through a statistical approach. In particular, the largest wavelength shift in a distribution of many events can be analytically related to the particle size, since this shift corresponds to binding directly on the lowest order polar mode (i.e., at the equator).[3] Unfortunately because of the statistical nature of this approach, one cannot be certain that the largest event in the distribution corresponds to a particle at the equator. Consequently, the size obtained is uncertain and many events are needed to generate the distribution.[4] Fortunately, there is another approach that avoids these difficulties, and that is what this paper is about.

The current idea is fully reactive, does not require mode splitting, and therefore can be applied in the weak coupling limit where the interaction g is considerably smaller than the linewidth, Γ, and the Q is modest ($<10^6$). However, like mode splitting, it involves the ratio of shifts from two different resonances in the same microcavity, and is therefore immune to long term temperature fluctuations. This approach involves the excitation of two resonances having the same angular momentum quantum number $\boldsymbol{l}$ but different m quantum numbers ($-l < m < l$) in a cavity for which a nanoparticle induced wavelength shift is much smaller than the linewidth (i.e., weak coupling). Although m is referred to as the magnetic quantum number in atomic physics, when considering different m modes within a microresonator having a given l, we will use the term polar modes. To understand what is involved, we must examine the shape of the polar WGM intensity. There are many such states that are characterized by $l-m+1$ intensity peaks along the polar direction. In a sphere, these m states are degenerate for a given angular momentum $\boldsymbol{l}$, but in a spheroid, this degeneracy is lifted, and the states separate spectrally. The first of these is an equatorial mode for which $m=l$, thereby producing one intensity peak centered about the equator (Fig. 1). The next with $m=l-1$ has two peaks, one to the North, and the other to the South of the equator (Fig. 1). It is important to realize that the two modes depicted in Fig. 1 are excited sequentially within the same slightly prolate microcavity by a fiber positioned slightly above or below the equator and directed along a line perpendicular to the symmetry axis of the spheroid. In what follows, we will show that the ratio of the resonance wavelength shifts of each of these modes provides a locator for the nano-particle's absolute latitude, from which its polarizability and size/mass may be estimated one event at a time (i.e., real time).

To start the description of the polar mode mechanism, we will first update the wavelength shift theory to include polar modes. For this purpose, we adopt the symbol $\Delta\lambda_{l,m}$ to describe the wavelength shift of a mode having an angular momentum number l, and polar number m. In what follows, we will show that the latitude angle for particle binding is easily obtained from the ratio of two wavelength shifts, $\Delta\lambda_{l,l-1}/\Delta\lambda_{l,l}$.

To understand the importance of polar modes in nanoparticle characterization, one simply has to return to the basic principle of microcavity reactive detection, the reactive

a)Author to whom correspondence should be addressed. Electronic mail: sarnold935@aol.com

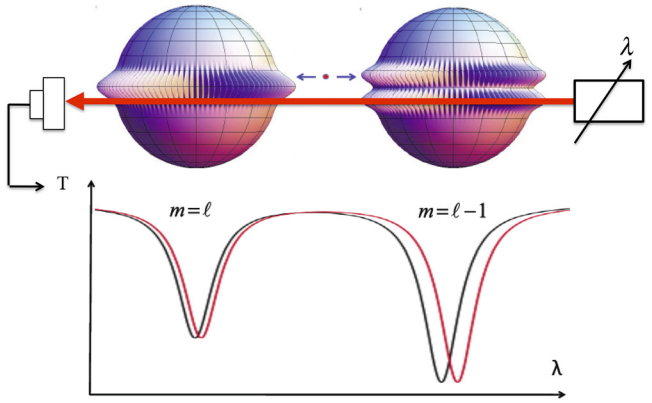

FIG. 1. Polar modes intensities of a single slightly prolate micro-spheroid excited sequentially during a spectral laser scan by a guided wave in a tapered fiber positioned just below the equator, and its corresponding transmission spectrum. The $m = l - 1$ mode on the right has a slightly longer resonance wavelength than the $m = l$ mode on the left. A nano-particle adsorbed north of the equator (red dot) has a larger overlap with the intensity of the $m = l - 1$ mode on the right, and consequently, this mode shifts (red curve) to a greater extent (above). The ratio of the two shifts for the same microcavity locates the nano-particle's latitude, from which its polarizability and size/mass are estimated.

sensing principle (RSP). The RSP simply states that "the perturbation in a resonator's photonic energy upon particle binding at $\boldsymbol{r}_p$ is equal to the energy required for the microcavity's reactive (evanescent) field $E_0(\boldsymbol{r}_p)$ to polarize the particle."[3] On this basis, the shift in resonance wavelength $\Delta\lambda$ is the wavelength λ times the ratio of the energy required to polarize the nanoparticle to the energy in the cavity. In a dipole approximation, the shift in wavelength[3]

$$\Delta\lambda \simeq \frac{\alpha_{ex} E_0^2(\boldsymbol{r}_p)}{2\int \varepsilon(r_c) E_0^2(\boldsymbol{r}_c) dV}\lambda, \tag{1}$$

where α_{ex} is the polarizability of the nanoparticle in excess of its environment (i.e., medium) and $\varepsilon(\boldsymbol{r}_c)$ is the permittivity of the cavity at position r_c. When applied to a homogeneous microsphere for $m \approx \boldsymbol{l} \gg \boldsymbol{1}$ (i.e., polar modes that resonate close to the equator), for a nanoparticle of radius a adsorbing on the surface, Eq. (1) becomes

$$\Delta\lambda_{l,m} \approx \frac{\alpha \left|Y_{l,m}(\xi_p)\right|^2 g(a/L)}{\left(n_s^2 - n_e^2\right)R^3}\lambda, \tag{2}$$

where $\alpha = \alpha_{ex}/\varepsilon_0$ is the "geometric" polarizability that is proportional to the volume of the nanoparticle ($\alpha = D_\alpha a^3$), R is the microsphere radius, L is the characteristic evanescent intensity length obtained from Mie theory, ξ_p is the latitude of the bound particle, n_s, n_e, and n_p are the refractive indices of the microsphere, environment, and nanoparticle, respectively, and finally, the constant $D_\alpha = 4\pi n_e^2(n_p^2 - n_e^2)/(n_p^2 + 2n_e^2)$. The form factor g corrects the simple point dipole theory (Eq. (1)) for a nanoparticle that is extended in size ($a \sim L$).[5] It is the overlap integral between the surface normalized evanescent intensity and volume elements of the nanoparticle divided by the volume of the particle. For a spherical nanoparticle, integration over its shape gives

$$g(z) = \frac{6}{(2z)^2}\left(1 + e^{-2z}\right) - \frac{12}{(2z)^3}\left(1 - e^{-2z}\right), \tag{3}$$

where $z = a/L$. The form factor has a simple limiting property, for $a \ll$ L, $g \simeq 1$. Eq. (2) is the key to our latitude locator.

Consider the ratio of wavelength shifts of the $m = l - 1$ to the $m = l$ modes at a latitude ξ_p; $\Delta\lambda_{l,l-1}(\xi_p)/\Delta\lambda_{l,l}(\xi_p)$. So long as the shifts are very small in comparison to the wavelength, from Eq. (2),

$$\frac{\Delta\lambda_{l,l-1}}{\Delta\lambda_{l,l}} = \frac{\left|Y_{l,l-1}(\xi_p)\right|^2}{\left|Y_{l,l}(\xi_p)\right|^2}. \tag{4}$$

As one can see that the right hand side of Eq. (4) only depends on the latitude ξ_p of the adsorbing particle, and consequently by placing experimental wavelength shift data on the left, this equation gives the latitude of the adsorbed nanoparticle independent of its physical properties, those of the resonator, or any refractive indices. Once ξ_p is determined, Eq. (2) can be used to calculate the size of the nanoparticle as well as the polarizability.

Our simple latitude locator equation (Eq. (4)) can be further simplified. As long as l is very large, and $l - m$ is very small, the spherical harmonic functions can be transformed to Hermite-Gauss asymptotic expressions[6] with the result that

$$\frac{\left|Y_{l,l-1}(\xi_p)\right|^2}{\left|Y_{l,l}(\xi_p)\right|^2} \approx 2(l-1)\xi_p^2. \tag{5}$$

Combining Eq. (4) with Eq. (5) gives the absolute latitude of the particle

$$|\xi_p| = \sqrt{\frac{1}{2(l-1)}\frac{\Delta\lambda_{l,l-1}}{\Delta\lambda_{l,l}}}. \tag{6}$$

With $|\xi_p|$ determined, the size a of the nanoparticle can be determined by re-expressing Eq. (2) as

$$a^3 g(a/L) \approx \frac{\left(n_s^2 - n_e^2\right)R^3}{\left|Y_{l,l}(\xi_p)\right|^2 D_\alpha}\frac{\Delta\lambda_{l,l}}{\lambda}. \tag{7}$$

The solution to Eq. (7) is particularly simple for $a \ll L$ since the form factor $g \simeq 1$ in this limit, and one gets a closed form algebraic solution. For larger particles, Eq. (3) is used for g and the resulting transcendental equation is solved numerically. Whether the particle is north or south of the equator has no relevance, since the square modulus of the spherical harmonic in the denominator of Eq. (7) is even with respect to the latitude.

To test our micro-latitude locator idea, we formed micro-spheroids by using CO_2 laser melting at the end of a tapered silica optical fiber (inset, Fig. 2). Shape analysis of the images revealed that our resonators were slightly prolate or oblate (eccentricity <3%). These silica micro-spheroids were then installed into our homemade microfluidic system,[7,8] where they were coupled to a tapered optical fiber. In the inset, the fiber is beneath the spheroid.

A typical under-coupled spectrum taken through the coupling fiber is shown in Fig. 2. All of the resonances were excited with a 1063 nm tunable Distributed Feedback (DFB) laser polarized along a meridian [Transverse Electric (TE) polarization]. The laser was current tuned with a saw tooth

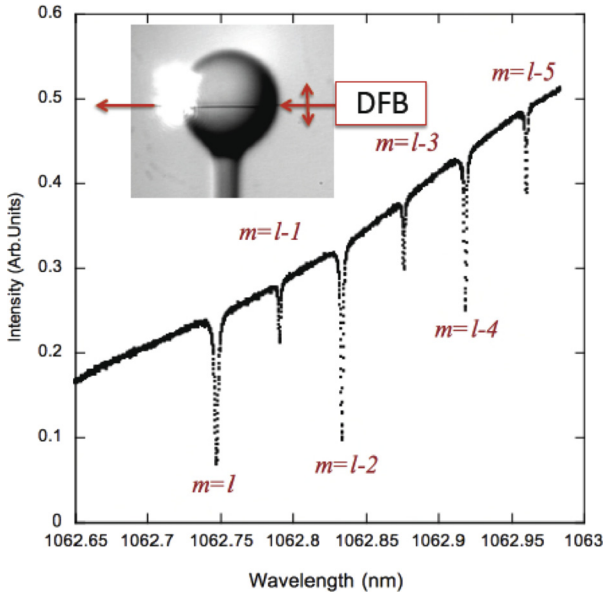

FIG. 2. Spectrum of a slightly prolate microcavity immersed in 30 mM NaCl solution and excited by tapered fiber coupling just below the equator as seen in the inset. The equatorial radius was 41 μm. From Mie theory, $l = 340$ with all modes having TE polarization. The DFB laser was scanned with a saw tooth drive having a period of 100 ms.

wave that accounts for the rising backbone of the spectrum. It should be noted that the resonance dip on the left has no neighbor at shorter wavelength. This is the signature of the $m = l$ equatorial mode of a prolate spheroid; the $m = l$ mode has the shortest wavelength.[9] To the right of this mode (longer wavelength) is the $m = l - 1$ mode which is narrower with a smaller dip. Note that the $m = l - 2$ mode is of similar depth to the $m = l$ mode and the $m = l - 3$ mode to longer wavelength looks similar in depth to the $m = l - 1$ mode. This sequence of deep-shallow-deep-shallow dips in Fig. 2 is a consequence of the overlap between the fiber field and the polar symmetries of the WGMs; the coupling constant requires performing volume integration over the product of the optical fiber field with the WGM field.[6] Whereas the $m = l$ mode is symmetric in latitude about the equator as is the fiber field, the $m = l - 1$ mode is asymmetric. Exciting the asymmetric WGM mode requires that the centerline of the exciting fiber be slightly above or below the equator. The fiber is placed in contact with the resonator to reduce mechanical vibration noise. This results in a red shift and broadening of the resonances. Upon coupling neither the $m = l$ or $m = l - 1$ resonances had Qs greater than 2×10^5.

The validity of the latitude locator idea was tested by injecting nanoparticles [polystyrene $\langle a_m \rangle \pm \sigma = 228 \pm 7$ nm from Polysciences] at a 20 fM concentration into our microfluidic system in the presence of the resonator depicted in Fig. 2. The solution had a 30 mM NaCl concentration to promote binding to the silica surface by decreasing the Debye length associated with ionized silanol groups.[10] Figure 3 shows data for two typical events. The event on the left appeared 874 s following the injection with a wavelength shift of 670 ± 5 fm for the $m = l$ mode and 410 ± 5 fm for the $m = l - 1$ mode. For the event on the right which occurred 2460 s after injection, the smaller shift occurred for the $m = l$ mode; 80 ± 7 fm as compared with 360 ± 7 fm for the $m = l - 1$ mode. For the former case, the latitude at which the nano-sphere attached from Eq. (6) in radians (degrees) is 0.078 ± 0.004 (1.72 ± 0.02 deg.). After numerically solving Eq. (6), we find the radius of this nanosphere to be 235.9 ± 0.2 nm. The latitude for the nanoparticle attachment on the right is 4.67 ± 0.26 degrees, and the radius from Eq. (6) is 217 ± 19 nm. Compared with the ensemble average from hydrosol manufacturer $\langle a_m \rangle \pm \sigma = 228 \pm 7$ nm, both results from our latitude locator approach overlap.

Table I shows the analysis of four recorded events. In all cases, the latitude locator results in the column marked a_p along with uncertainties are calculated from Eqs. (6) and (7) by using the wavelength shift measurement and their uncertainties. For example, the relatively large uncertainty arrived for a_p in the third event is a direct result of the large fractional experimental uncertainty in $\Delta\lambda_{340,340}$ for this event. It should be noted that the results for a_p including uncertainties overlap the manufacturer's ensemble measurements in the last column.

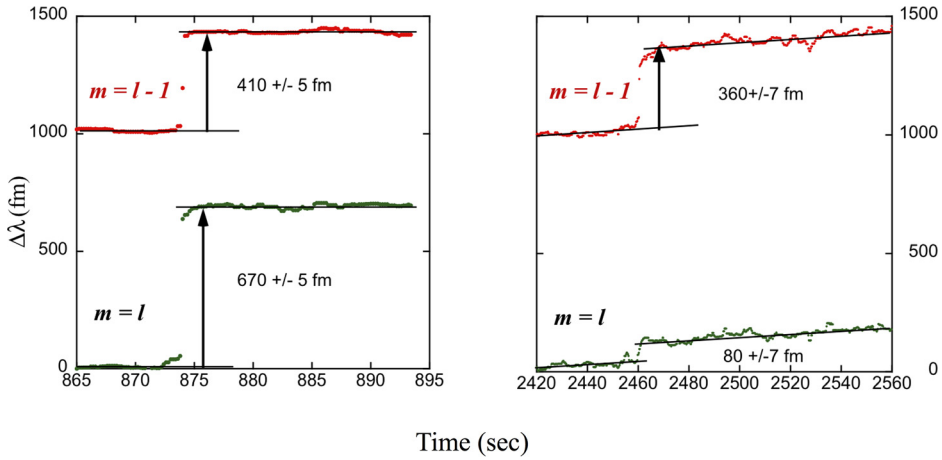

FIG. 3. Two event recordings of the $m = l$, $m = l - 1$, modes for signaling the binding of two polystyrene nano-spheres to the micro-spheroid in Fig. 2. For each event, an offset of 1000 fm between the $m = l$ and $m = l - 1$ modes was chosen for clarity. The particles used are reported by the manufacturer (Polysciences) as having an ensemble radius $\langle a_m \rangle = 228$ nm with a standard deviation of 7 nm. For the binding event on the left near 874 s, $\Delta\lambda_{l,l} > \Delta\lambda_{l,l-1}$. The opposite is true for the binding even on the right near 2460 s. Although the $m = l$ event on the left demonstrates a shift of 700% greater than that on the right, the differences in the radii arrived at from Eqs. (6) and (7) is less than 8%. These results as well as others are listed in Table I.

TABLE I. The analysis of 4 events following the injection of polystyrene nano-spheres from a manufactured hydrosol (Polysciences) having an ensemble mean radius $\langle a_m \rangle = 228$ nm with a standard deviation of $\sigma = 7$ nm. The microcavity was the one in Fig. 2. Each of the particle radii a_p in the 5th column are determined only from the data for the associated event using Eqs. (6) and (7). The refractive indices n_s, n_e, and n_p were taken as 1.449, 1.326, and 1.572, respectively.

Event	$\Delta\lambda_{340,340}$ (fm)	$\Delta\lambda_{340,339}$ (fm)	$\lvert\xi_p\rvert$ (deg) using Eq. (6)	a_p (nm) using Eq. (7)	$\langle a_m \rangle \pm \sigma$ (nm)
1. 600 s	800 ± 5	40 ± 5	0.49 ± 0.03	224.5 ± 0.3	228 ± 7
2. 874 s	670 ± 5	410 ± 5	1.72 ± 0.02	235.9 ± 0.2	228 ± 7
3. 2460 s	80 ± 7	360 ± 7	4.67 ± 0.26	217 ± 19	228 ± 7
4. 3860 s	150 ± 5	520 ± 5	4.10 ± 0.09	228.8 ± 4.2	228 ± 7

There is no doubt that the use of the latitude locator produces a much more accurate size for a single event than simply assuming that particles bind to the equator. Wavelength shifts associated with a given resonance (e.g., $m = l$ or $m = l - 1$) vary by a factor of ~10 (1000%) in Table I, leading to size estimates based on the assumption of equatorial binding that vary by a factor of $\sim 10^{1/3}$. That is over 200%. However, with the latitude locator to determine the polar location, this uncertainty is severely reduced as seen in Table I (e.g., for events 1 and 2, propagating the measurement uncertainties through Eqs. (6) and (7) produces size uncertainties ~1%).

Although our major goal in this Letter is to outline the latitude locator idea, we imagine its major use to be in measuring the size distribution in a heterogeneous solution in which each binding event counts. To test this notion, we added 178 nm PS beads to 228 nm PS beads we had used previously. Figure 4 shows the binding curves recorded for the $m = l$ and $m = l - 1$ modes. The latitude locator combined with Eq. (7) easily identified two particle ranges, 231 to 250 nm, and 167 to 174 nm.

We have not been concerned with the issue of characterizing an ultra-small particle, since that has already been done using the resonance shift in the statistical manner by looking for the largest wavelength shift in a distribution of events.[4] The authors of Ref. 4 show that it is possible to sense a particle with a radius down to 12.5 nm in aqueous solution using a scanning technique. The latitude locator principle should enable this to be done deterministically, and in one event.

Although we have confined our attention to microspheroidal resonators, the same principle can be used for detection by other WGM shapes. Similar m modes have been identified in rolled up cylinders[11] and micro-toroids,[9] although multiple m modes have not been used for precise nanoparticle sizing with these designs.

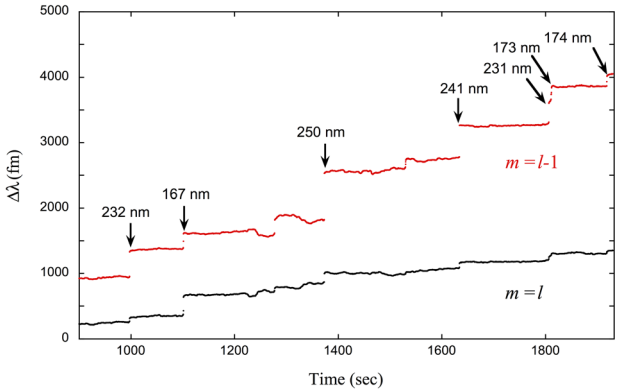

FIG. 4. Experimental binding curves on a 41μm radius slightly prolate spheroid recorded for the $m = l$ and $m = l - 1$ modes. The solution contained PS nanospheres (mixture) having manufactured ensemble radii of 178 ± 7 and 228 ± 7. The numbers at the beginning of each binding event is the computed radius for that event based on Eqs. (6) and (7).

The research described herein was supported by the National Science Foundation Grant EECS 1303499. We thank W.W. Langbein for pointing out that the approximation leading to Eq. (5) is for small latitudes such as those in this paper.

[1]J. Zhu, S. K. Ozdemir, Y. F. Xiao, L. Li, L. He, D. R. Chen, and L. Yang, Nat. Photonics **4**, 46 (2010).
[2]W. Kim, S. K. Ozdemir, J. Zhu, and L. Yang, Appl. Phys. Lett. **98**, 141106 (2011).
[3]S. Arnold, M. Khoshsima, I. Teraoka, S. Holler, and F. Vollmer, Opt. Lett. **28**, 272 (2003).
[4]T. Lu, H. Lee, T. Chen, S. Herchak, J. H. Kim, S. E. Fraser, R. C. Flagan, and K. Vahala, Proc. Natl. Acad. Sci. USA **108**, 5976 (2011).
[5]F. Vollmer, "Resonant detection of nano to microscopic objects using whispering gallery modes," Ph.D. dissertation (Rockefeller University, 2004).
[6]B. E. Little, J. P. Laine, and H. A. Haus, J. Lightwave Technol. **17**, 704 (1999).
[7]S. Arnold, R. Ramjit, D. Keng, V. Kolchenko, and I. Teraoka, Faraday Discuss. **137**, 65 (2008).
[8]D. Keng, S. R. McAnanama, I. Teraoka, and S. Arnold, Appl. Phys. Lett. **91**, 103902 (2007).
[9]G. Lin, B. Qian, F. Orucevic, Y. Candela, J. B. Jager, Z. Cai, V. Lefevre-Segun, and J. Hare, Opt. Lett. **35**, 583 (2010).
[10]S. Arnold, D. Keng, S. I. Shopova, S. Holler, W. Zurawsky, and F. Vollmer, Opt. Express **17**, 6230 (2009).
[11]S. Li, L. Ma, H. Zhen, M. R. Jorgensen, S. Kiravittaya, and O. G. Schmidt, Appl. Phys. Lett. **101**, 231106 (2012).